High-Resolution Single Photon Level Storage of Telecom Light Based on Thin Film Lithium Niobate Photonics

Ekici, Çağın; Yu, Yonghe; Adcock, Jeremy C.; Muthali, Alif Laila; Tan, Heyun; Lin, Zhongjin; Li, Hao; Oxenløwe, Leif Katsuo; Cai, Xinlun; Ding, Yunhong

Published in:
Advanced Quantum Technologies

Link to article, DOI:
10.1002/qute.202300195

Publication date:
2024

Document Version
Peer reviewed version

ADVANCED QUANTUM TECHNOLOGIES
www.advquantumtech.com

High-Resolution Single Photon Level Storage of Telecom Light Based on Thin Film Lithium Niobate Photonics

Çağın Ekici, Yonghe Yu, Jeremy C. Adcock, Alif Laila Muthali, Heyun Tan, Zhongjin Lin, Hao Li, Leif Katsuo Oxenløwe, Xinlun Cai, and Yunhong Ding**

This study presents an experimental analysis of high-resolution single photon buffers based on low-loss thin film lithium niobate (TFLN) photonic devices operating at room temperature. While dynamically controlling writing and reading operations within picosecond timescales poses a challenge, the devices are capable of resolving 102.8 ± 4.6 ps time step with -0.89 dB loss per round-trip and 197.7 ± 6.6 ps time steps with -1.29 dB loss per round-trip, respectively. These results imply that the devices are at the cutting edge of on-chip technology, performing in the current state of the art at the single photon level. Both of the single photon buffers do not introduce any detrimental effects and provide a high signal-to-noise ratio (SNR). The room-temperature, low-loss, and voltage-controlled TFLN buffers combine scalable architecture with relatively high buffering capacity in the sub-nanosecond regime and are expected to unlock many novel photonics applications such as temporally multiplexed single photon sources.

1. Introduction

Quantum photonic memories are crucial for quantum information science, where they can be exploited as a bridge between photonic systems operating at different speeds to facilitate synchronization.[1,2] For example, they can be used to optimize two-photon interference from distant sources in a quantum network,[3,4] to buffer gates of probabilistic nature, and to convert photon pair sources to on-demand photon sources through time-bin multiplexing.[5,6] The buffers, furthermore, can also be utilized to temporally stagger photons so that detrimental interference effects in specific parts of the network are circumvented. To date, optical buffers based on recirculating loops,[7] slow-light,[8] coupled resonator optical waveguides,[9] and Bragg scattering four-wave mixing[10] have been reported. However, all these techniques either have an excessive loss that make them unsuitable for quantum photonic implementations or rely on complicated experimental setups, e.g., relying on several nonlinear processes to take place.[11]

The main contenders to these all optical solutions are media-based quantum photonic memories (MBQPM), which utilize atom-photon interaction featuring the reversible mapping of quantum states of light onto matter.[12] However, they suffer from several drawbacks, such as requiring cryogenic temperatures,[13] are technically challenging to implement, and generally operate at specific wavelengths, i.e., have severely limited bandwidth. Another issue with the MBQPM is that photon retrieval is a challenging process, resulting in a lower efficiency.[14] Furthermore, they generally have time-bin resolution in the order of several nanoseconds, rather than picoseconds. Operating in the picosecond regime can be useful in applications such as time-bin multiplexing of photon pair sources, as higher speeds equate to lower single photon losses.

Since MBQPM approaches increase the complexity of the quantum systems, they hinder the practicality and scalability of the experiments. The natural candidate to overcome this issue is an entirely integrated photonic-based realizations, which are expected to play a crucial role quantum photonic technology as it develops from few-qubit architectures to systems processing hundreds of qubits.[15–17] These platforms offer remarkable advantages, such as enhancements in efficiency, robustness, while many integrated photonic platforms have been used to

Ç. Ekici, Y. Yu, J. C. Adcock, A. L. Muthali, L. K. Oxenløwe, Y. Ding
Center for Silicon Photonics for Optical Communication (SPOC)
Department of Electrical and Photonics Engineering
Technical University of Denmark
Lyngby 2800, Denmark
E-mail: caek@dtu.dk; yudin@dtu.dk

J. C. Adcock
Big Photon Lab, H. H. Wills Physics Laboratory & Department of Electrical and Electronic Engineering
University of Bristol
Tyndall Ave, Bristol BS8 1FD, UK

H. Tan, H. Li, X. Cai
State Key Laboratory of Optoelectronic Materials and Technologies
School of Electronics and Information Technology
Sun Yat-sen University
Guangzhou 510275, China

Z. Lin
Department of Electrical and Computer Engineering
The University of British Columbia
Vancouver, BC V6T 1Z4, Canada

The ORCID identification number(s) for the author(s) of this article can be found under https://doi.org/10.1002/qute.202300195

DOI: 10.1002/qute.202300195

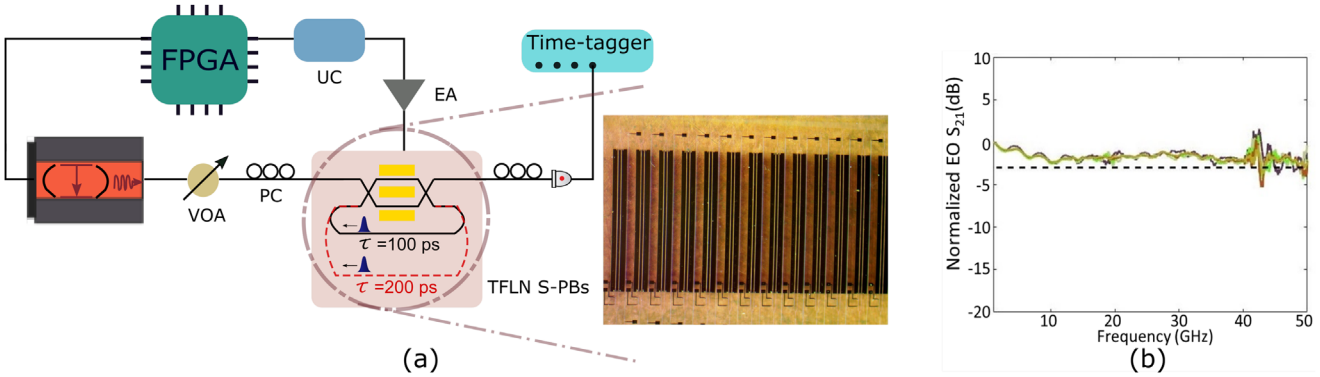

Figure 1. a) Schematics of the experimental setup of two recirculating 100 ps loop and 200 ps loop with a optical micrograph of the TFLN chip (100 ps loops). b) Electro-optic bandwidth (S_{21}) measurement. Abbreviations: FPGA: Field-Programmable Gate Array, VOA: Variable Optical Attenuator, PC: Polarization Controller, UC: Ultrafast Comparator, EA: Electronic Amplifier, TFLN S-PB: TFLN Single Photon Buffer.

demonstrate quantum information processing capability.[18] Among them, the silicon photonic platform of particular importance and is the subject of numerous quantum applications.[19] Recently, high-resolution silicon on-chip single photon buffer-based on voltage driven microdisc resonator in the add-drop configuration with -0.72 dB/100 ps has been demonstrated, however the system can only be controlled with 200 ps time steps.[20] The TFLN platform, on the other hand, has emerged as a strong contender with a unique set of capabilities for high-speed, low-loss applications.[21–23] Additionally, lithium niobate (LN) is an excellent crystalline host for rare-earth ions, making it one of the best candidates for on-chip quantum memories.[24] Notably, erbium (Er) doped LN exhibits coherence times on the order of microseconds (μs), essential for achieving sufficient storage times and high-efficiency storage for multiple temporal modes. In addition, it allows for a compatible interface between the memory and fiber-based communication systems, thanks to the 1.5 μm transition of Er ions.[25]

In this paper, we experimentally demonstrate on-chip TFLN single photon buffers implementing high-speed, low-loss, and voltage-controlled interferometric switching, embracing the requirements for a scalable high-resolution single photon buffer. We demonstrate two TFLN-based buffers featuring recirculating loops controlled by high-speed and low-loss switches. The first features a 1.4 cm-long loop with a round-trip time of $\tau_1 = 102.8 \pm 4.6$ ps, and the second features a 2.8 cm-long loop with round-trip time of $\tau_2 = 197.7 \pm 6.6$ ps. Both allow the storage of photonic states with a resolution of their characteristic storage time τ_i, up to $14\tau = 1.4$ ns and $9\tau = 1.8$ ns, with internal storage efficiencies of 5.3% and 6.3%, respectively. The presented buffers can be further exploited to process time-bin encoded quantum information at higher rates. Recently, quantum computational advantage has been demonstrated by utilizing the similar building blocks, i.e., fiber-based recirculating loops, but at a much slower rate.[26]

2. Device Design and Characterization

The design of the proposed device is based on a commercial TFLN platform, which consists of a 360 nm thick x-cut LN thin film to exploit the largest electro-optic tensor component r_{33} of LN, satisfying single transverse mode operation at telecommunication band, on a 500 μm thick quartz handle with a 2 μm thick buried SiO_2 in between. In addition, using x-cut TFLN allows to design the traveling wave electrodes of the modulator to be on the sides of the waveguides and be simply fabricated by lithography and liftoff process. The devices include a high-speed optical switch and an optical delay line (**Figure 1**a). To achieve a large bandwidth, we use capacitance-loaded traveling-wave electrodes with a length of 4 mm. Further details of this design can be found in ref. [27]. We characterize the electro-optic response of the fabricated device at a telecom wavelength of 1550 nm, using a vector network analyzer (Agilent N5227A) and find that the switches exhibit a 3-dB electro-optic bandwidth more than 40 GHz (Figure 1b). The measured fiber-to-fiber insertion loss is less than -6.2 dB (including coupling loss).

3. Experimental Setup and Results

The measurements are carried out on devices under test with a loop round-trip time of 102.8 ± 4.6 ps and 197.7 ± 6.6 ps, using the experimental setup illustrated in Figure 1a. Weak coherent pulses (1550 nm, 16 ps pulse duration) with off-chip average photon number of $\mu = 0.3$ are injected into the devices with 100 MHz repetition rate (the relatively slow repetition rate prevents single photon detectors being saturated). The utilization of weak coherent pulses is due to the their practicality and cost-effectiveness in generating pulses probabilistically at the single photon level. These states have found extensive application in various areas, including quantum key distribution systems,[28] testing single photon detectors,[29,30] characterizing quantum memories via coherent-state quantum process tomography,[31] and characterizing single photon level storages.[11]

Electrical signals, generated via an FPGA, control the interferometric switch for storage and retrieval operations. The electrical controlling signals are fed into an ultrafast comparator to obtain a fast fall-rise time and further amplified to match the V_π of the TFLN switch before being applied to the device through high speed radio frequency probe arms via micropositioners. After a given storage and retrieval delay, photons are detected by a superconducting nanowire single photon detector (SNSPD) and recorded by a time-tagger (TT) to produce a real-time histogram of the detection event.

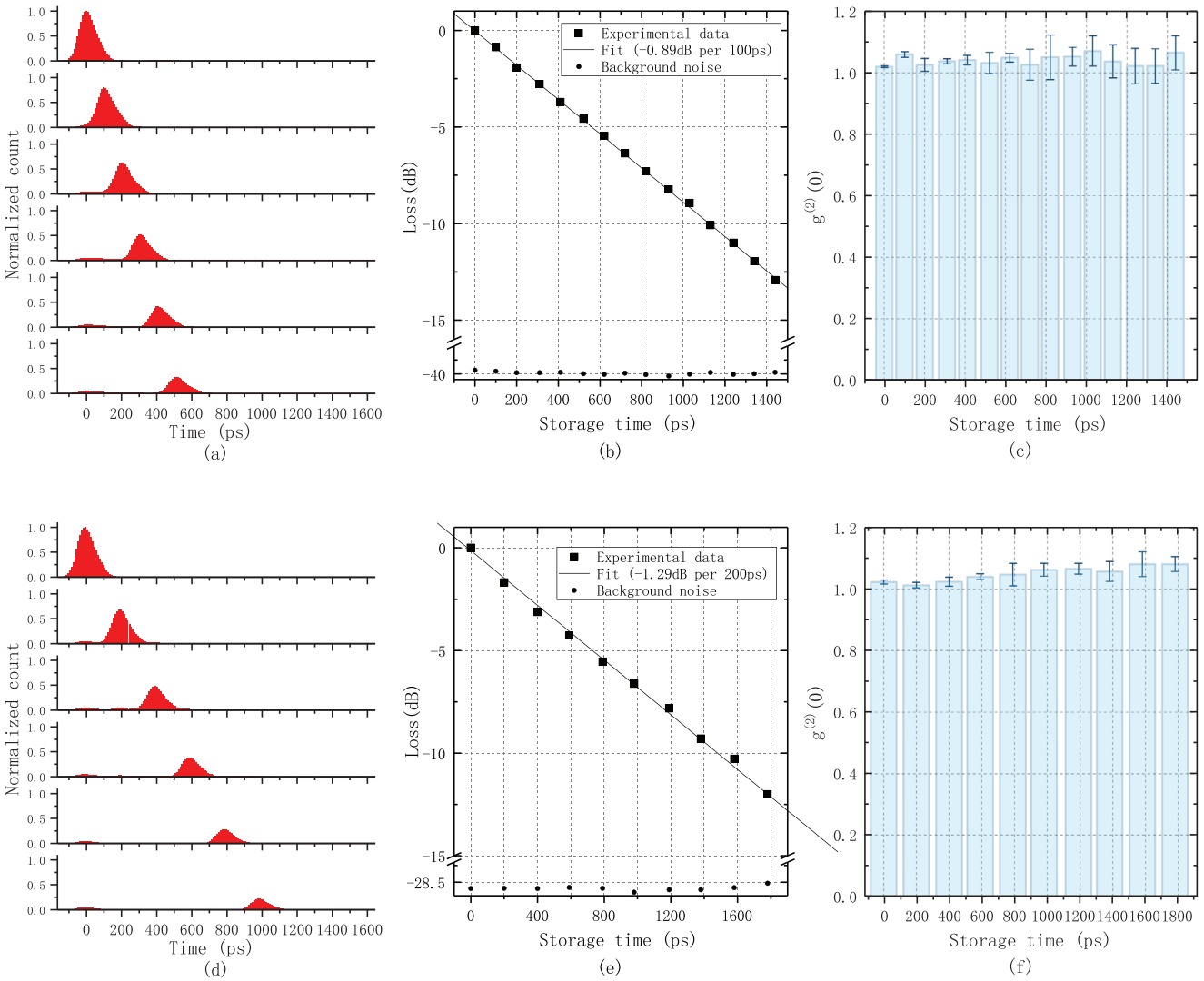

Figure 2. Single photon level storage in the $\tau = 100$ ps device: a) Normalized histogram counts as a function of storage time. b) The peak amplitudes of the normalized histogram counts. A linear fit reveals a loss of −0.89 dB/100 ps. c) second order correlation function $g^{(2)}(0)$ of the read-out single photons for different storage times. Single photon level storage in the $\tau = 200$ ps device: d) Normalized histogram counts as a function of storage time. e) The peak amplitudes of the normalized histogram counts. A linear fit reveals a loss of −1.29 dB/200 ps. f) second order correlation function $g^{(2)}(0)$ of the read-out single photons for different storage times.

The experimental results of single photon level storage with our TFLN chip are shown in **Figure 2**. Normalized histogram counts for the reference pulse (no round-trip) and the first five round trips are depicted in Figure 2a and in Figure 2d for illustrative purposes for 100 ps and 200 ps time steps, respectively. The storage loss performance of the single photon buffers as a function of storage time are exhibited in Figure 2b,e. Each peak value after a round-trip has been fitted the line with a slope −0.89 dB for a length of 1.4 cm and the line with a slope −1.29 dB for a length of 2.8 cm. This implies a −0.28 $dBcm^{-1}$ loss in the waveguide part, −0.51 dB loss in the interferometer region.

The measured background noise floors are shown by the dotted lines in Figure 2b,d, demonstrating a high SNR value. Subsequently, in order to demonstrate that our buffers do not introduce factors such as thermal noise, random phase modulation, or other decoherence processes that might negatively impact the system, we measure the second-order correlation function $g^{(2)}(0)$ by introducing a 50/50 fiber optic beam splitter before the detection. The results are depicted in Figure 2c,f. $g^{(2)}(0)$ remains approximately constant at around *one* for each round-trip, indicating the absence of any detrimental effects. In addition, even though the presence of loss leads to an overall reduction in the signal strength, the distributions still follow a Poisson distribution. However, in Figure 2f, $g^{(2)}(0)$ shows a slight increase. This observation can be attributed to the fact that $g^{(2)}(0)$ increases as the signal component decreases and the noise component increases. The deviation from the optimal situation might be observed in Figure 2e as background noise exhibits a positive slope toward the end of the storage.

In addition, for a comprehensive assessment of pulse dispersion and distortion, our buffers are illuminated with a high-intensity laser pulse (pulse duration of 16 ps, average power

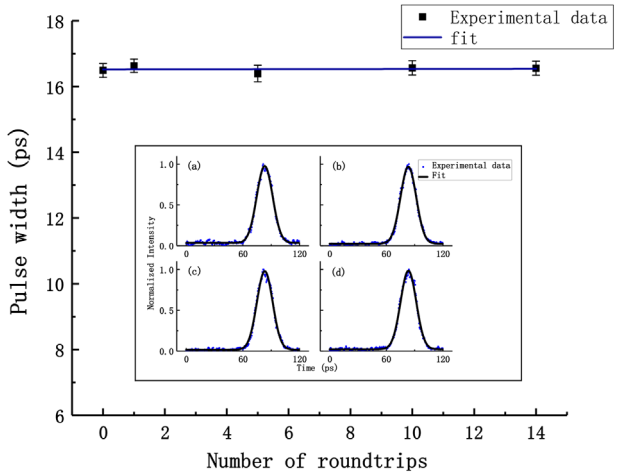

Figure 3. Autocorrelation results obtained from the 200 ps device for various round trips: 0, 1, 5, 10, and 14. The inset plot displays the experimental data along with the corresponding Gaussian fits for different round trips a) 1, b) 5, c) 10, d) 14. The widths of these Gaussian fits are depicted as a function of round trips, ≈ 16.3 ps.

P_{avg}=12 dBm, and a repetition rate of 100 MHz) to conduct autocorrelation measurements (on the 200 ps device) as a function of round-trip. The findings in **Figure 3** demonstrate the robustness of the system. The inset plots in Figure 3 provide a closer view of the experimental data along with the corresponding Gaussian fits for different round trips: a) 1 round-trip, b) 5 round trips, c) 10 round trips, and d) 14 round trips. Notably, even after 14 round trips—equivalent to a propagation distance of approximately 40 cm—pulse broadening effects are negligible. Furthermore, the switching process itself does not introduce any observable pulse distortion. These outcomes indicate the stability and fidelity of our system, which is a crucial figure of merit in the context of numerous quantum implementations, particularly those reliant on the indistinguishability of photons, such as quantum interference.

Note that, in Figure 2a,d the extinction ratio between reference pulse and leakage in the reference (0^{th}) time-bin is 14 dB. Furthermore, the broadened widths of the observed distributions can be attributed to the jitter introduced by the detection electronics. The effects of the SNSPD and the TT become apparent in the broadened distributions.

Table 1 provides an overview of integrated devices designed for single photon (level) storage, highlighting key representative results such as storage efficiency (SE), i.e., the ratio of retrieved photons to the stored input photons, and resolution. This comparison emphasizes the need for a storage medium featuring resolution on the order of picoseconds with increased SE.

4. Outlook

LN photonics is very dynamic area of research and is poised for a broad range of applications from signal processing to burgeoning quantum technology. However, propagation loss is a limiting factor. Therefore, significant efforts have been made to reduce loss, with major gains in recent demonstrations down to a state of the art of −0.027 $dBcm^{-1}$.[35–37] In parallel with this, the group-velocity

Table 1. Integrated Photonics Devices for Single Photon (Level) Optical Buffers/Memories.

Material	Delay	Resolution	SE (%)
SOI[20]	1.2 ns	100 ps*	13.8
SOI[20]	1.2 ns	200 ps	1.2
Er:$LiNbO_3$[25]	200 ns	200 ns	2.83
Ti:Tm:$LiNbO_3$[32]	7 ns	7 ns	2
Eu:Y_2SiO_5[33]	1 µs	0.5 µs	15.8
Pr:Y_2SiO_5[34]	5.5 µs	0.5 µs	1
TFLN [This Work]	1.4 ns	100 ps	5.3
TFLN [This Work]	1.8 ns	200 ps	6.3

*: Can only be controlled with 200 ps time steps.

dispersion (GVD) is a primary concern, as it leads to distinguishability between pulses, which are stored for different durations. In simulation, the GVD of our TFLN loop is found to be $|D| \approx 400$ ps/(nm-km), meaning that an initially unchirped 15 ps duration pulse disperses by approximately 0.001 ps after 1 cm of propagation, which is insignificant for both our loops. As an alternative, one can also take the condition for a slow-light buffer into account relating the maximum allowable length L and bit rate B[38]:

$$|\beta_2| B^2 L < \frac{1}{16 \log 2} \quad (1)$$

where the second order dispersion, β_2, is the GVD. Considering $\beta_2 = 5.1 \times 10^{-25}$ s^2m^{-1} of our structure and a bit rate of $B = 10^{10}$ Hz, L is found to be ≈ 1.7 km. This implies that over the length scales of interest, pulse broadening effects can only become visible when increasing the number of round trips by many orders of magnitude, as it is demonstrated experimentally in Figure 3.

One of the most demanding characteristics of single photon buffers is high SE, which is upper bounded by the loss. Another important figure of merit directly related to the SE is the delay-bandwidth product (DBP) (or the storage time-bandwidth product) indicating the capacity of the device to buffer photonic pulses into different time bins. This is defined as the product of the delay time at 50% storage efficiency and the bandwidth of the input pulse.[39,40] The achieved DBP ≈ 11 for both our buffers suggesting that time-bin multiplexing of photon pair (signal and idler) sources may be possible using our buffers. The key idea of time-bin multiplexing is to exploit heralding (detection of idler photon) to actively store and route the heralded photon (signal) to a predetermined output time-bin.[41] This makes low-loss storage a critical ingredient. Hence, our devices can effectively function as a storage medium for signal photons generated by pulsed lasers operating at a repetition rate in the GHz regime. They are capable of catching and releasing signal photons discretely with 100 ps and 200 ps time steps triggered by electrical signals from idler photon detection events.[5] For instance, for a round-trip storage efficiency r_{se} of 0.82 (100 ps device), a photon generated in the 36^{th} time-bin must traverse the loop 36 times, resulting in a photon survival probability of only 1.3%, which is not significant. While for r_{se}=0.74 (200 ps device) a photon generated in 12^{th} time-bin survives with probability of only 2.6%, which can also be ignored. On the other hand, with state-of-the-art waveguide loss (−0.027

dBcm^{-1}), SE would significantly increase, potentially resulting in DBP that could reach up to 100. This would allow hundreds of time-bins to be effectively multiplexed, resulting in a near-deterministic multiplexed single photon source. Moreover, this improvement in SE would further boost the time-bin encoded architectures to accomplish quantum computational advantage without compromising on universality.[42]

5. Conclusion

Integrated photonics provide an extremely promising pathway for the development of large-scale quantum systems thanks to their compact size, high stability and ease of packaging. Meanwhile, dynamic quantum photonic circuits featuring feed forward, such as multiplexed single photon source and entanglement heralding, hold the key to large-scale quantum photonics systems. In this work, we have experimentally demonstrated TFLN single photon buffers based on recirculating loops which offer high SNR, low-loss and discrete time-bin buffering capacity (DBP). This is a crucial stepping stone toward feed forward quantum photonics systems, and eventually large-scale quantum photonics technology.

Acknowledgements

Ç.E. and Y.Y. contributed equally to this work. The authors acknowledged funding from Villum Fonden Young Investigator project QUANPIC (Ref. 00025298) and Danish National Research Foundation Center of Excellence, SPOC (Ref. DNRF123).

Conflict of Interest

The authors declare no conflict of interest.

Data Availability Statement

The data that support the findings of this study are available from the corresponding author upon reasonable request.

Keywords

electro-optic devices, integrated quantum photonics, single photon buffer

Received: June 29, 2023
Revised: September 9, 2023
Published online:

[1] A. I. Lvovsky, B. C. Sanders, W. Tittel, *Nat. Photonics* **2009**, *3*, 706.
[2] K. Makino, Y. Hashimoto, J.-i. Yoshikawa, H. Ohdan, T. Toyama, P. van Loock, A. Furusawa, *Sci. Adv.* **2016**, *2*, e1501772.
[3] K. Azuma, K. Tamaki, H.-K. Lo, *Nat. Commun.* **2015**, *6*, 6787.
[4] M. K. Bhaskar, R. Riedinger, B. Machielse, D. S. Levonian, C. T. Nguyen, E. N. Knall, H. Park, D. Englund, M. Lončar, D. D. Sukachev, M. D. Lukin, *Nature* **2020**, *580*, 60.
[5] J. C. Adcock, D. Bacco, Y. Ding, *Quant. Sci. Technol.* **2022**, *7*, 025025.
[6] J. C. Adcock, D. Bacco, Y. Ding, in *CLEO: Applications and Technology*, Optica Publishing Group, Washington, DC **2022**, p. JTu3B–1.
[7] E. F. Burmeister, D. J. Blumenthal, J. E. Bowers, *Opt. Switch. Netw.* **2008**, *5*, 10.
[8] Y. Okawachi, M. S. Bigelow, J. E. Sharping, Z. Zhu, A. Schweinsberg, D. J. Gauthier, R. W. Boyd, A. L. Gaeta, *Phys. Rev. Lett.* **2005**, *94*, 153902.
[9] H. Takesue, N. Matsuda, E. Kuramochi, W. J. Munro, M. Notomi, *Nat. Commun.* **2013**, *4*, 2725.
[10] S. Clemmen, A. Farsi, S. Ramelow, A. L. Gaeta, *Opt. Lett.* **2018**, *43*, 2138.
[11] K. A. G. Bonsma-Fisher, C. Hnatovsky, D. Grobnic, S. J. Mihailov, P. J. Bustard, D. G. England, B. J. Sussman, *arXiv:2303.12794* **2023**.
[12] L. Ma, O. Slattery, X. Tang, *J. Res. Natl. Inst. Stand. Technol.* **2020**, *125*, 125002.
[13] J. Jin, E. Saglamyurek, V. Verma, F. Marsili, S. W. Nam, D. Oblak, W. Tittel, *Phys. Rev. Lett.* **2015**, *115*, 140501.
[14] A. Holzäpfel, J. Etesse, K. T. Kaczmarek, A. Tiranov, N. Gisin, M. Afzelius, *New J. Phys.* **2020**, *22*, 063009.
[15] J. C. Adcock, Y. Ding, *Front. Optoelectron.* **2022**, *15*, 7.
[16] G. Moody, V. J. Sorger, D. J. Blumenthal, P. W. Juodawlkis, W. Loh, C. Sorace-Agaskar, A. E. Jones, K. C. Balram, J. C. Matthews, A. Laing, M. Davanco, L. Chang, J. E. Bowers, N. Quack, C. Galland, I. Aharonovich, M. A. Wolff, C. Schuck, N. Sinclair, M. Lončar, T. Komljenovic, D. Weld, S. Mookherjea, S. Buckley, M. Radulaski, S. Reitzenstein, B. Pingault, B. Machielse, D. Mukhopadhyay, A. Akimov, et al., *J. Phys.: Photonics* **2022**, *4*, 012501.
[17] S. Saravi, T. Pertsch, F. Setzpfandt, *Adv. Opt. Mater.* **2021**, *9*, 2100789.
[18] J. Wang, F. Sciarrino, A. Laing, M. G. Thompson, *Nat. Photonics* **2020**, *14*, 273.
[19] J. C. Adcock, J. Bao, Y. Chi, X. Chen, D. Bacco, Q. Gong, L. K. Oxenløwe, J. Wang, Y. Ding, *IEEE J. Sel. Top. Quantum Electron.* **2020**, *27*, 1.
[20] X. Wang, S. Mookherjea, *Chip* **2022**, *1*, 100028.
[21] M. Bazzan, C. Sada, *Appl. Phys. Rev.* **2015**, *2*, 040603.
[22] Z. Lin, Y. Lin, H. Li, M. Xu, M. He, W. Ke, H. Tan, Y. Han, Z. Li, D. Wang, X. S. Yao, S. Fu, S. Yu, X. Cai, *Light: Sci. Appl.* **2022**, *11*, 93.
[23] W. Ke, Y. Lin, M. He, M. Xu, J. Zhang, Z. Lin, S. Yu, X. Cai, *Photonics Res.* **2022**, *10*, 2575.
[24] Y. Jia, J. Wu, X. Sun, X. Yan, R. Xie, L. Wang, Y. Chen, F. Chen, *Laser Photonics Rev.* **2022**, *16*, 2200059.
[25] X. Zhang, B. Zhang, S. Wei, H. Li, J. Liao, C. Li, G. Deng, Y. Wang, H. Song, L. You, B. Jing, F. Chen, G. Guo, Q. Zhou, *Sci. Adv.* **2023**, *9*, eadf4587.
[26] L. S. Madsen, F. Laudenbach, M. F. Askarani, F. Rortais, T. Vincent, J. F. Bulmer, F. M. Miatto, L. Neuhaus, L. G. Helt, M. J. Collins, A. E. Lita, T. Gerrits, S. Woo Nam, V. D. Vaidya, M. Menotti, I. Dhand, Z. Vernon, N. Quesada, J. Lavoie, *Nature* **2022**, *606*, 75.
[27] M. Xu, Y. Zhu, F. Pittalà, J. Tang, M. He, W. C. Ng, J. Wang, Z. Ruan, X. Tang, M. Kuschnerov, L. Liu, S. Yu, B. Zheng, X. Cai, *Optica* **2022**, *9*, 61.
[28] T. K. Paraïso, R. I. Woodward, D. G. Marangon, V. Lovic, Z. Yuan, A. J. Shields, *Adv. Quantum Technol.* **2021**, *4*, 2100062.
[29] T. F. Da Silva, G. B. Xavier, J. P. Von Der Weid, *IEEE J. Quantum Electron.* **2011**, *47*, 1251.
[30] G. Humer, M. Peev, C. Schaeff, S. Ramelow, M. Stipčević, R. Ursin, *J. Lightwave Technol.* **2015**, *33*, 3098.
[31] M. Lobino, C. Kupchak, E. Figueroa, A. Lvovsky, *Phys. Rev. Lett.* **2009**, *102*, 203601.
[32] E. Saglamyurek, N. Sinclair, J. Jin, J. A. Slater, D. Oblak, F. Bussieres, M. George, R. Ricken, W. Sohler, W. Tittel, *Nature* **2011**, *469*, 512.
[33] C. Liu, T.-X. Zhu, M.-X. Su, Y.-Z. Ma, Z.-Q. Zhou, C.-F. Li, G.-C. Guo, *Phys. Rev. Lett.* **2020**, *125*, 260504.

[34] A. Seri, G. Corrielli, D. Lago-Rivera, A. Lenhard, H. de Riedmatten, R. Osellame, M. Mazzera, *Optica* **2018**, *5*, 934.
[35] C. Wang, M. Zhang, X. Chen, M. Bertrand, A. Shams-Ansari, S. Chandrasekhar, P. Winzer, M. Lončar, *Nature* **2018**, *562*, 101.
[36] M. Zhang, C. Wang, R. Cheng, A. Shams-Ansari, M. Lončar, *Optica* **2017**, *4*, 1536.
[37] J. Lin, F. Bo, Y. Cheng, J. Xu, *Photonics Res.* **2020**, *8*, 1910.
[38] J. B. Khurgin, *Adv. Opt. Photonics* **2010**, *2*, 287.
[39] Y.-H. Chen, M.-J. Lee, I.-C. Wang, S. Du, Y.-F. Chen, Y.-C. Chen, A. Y. Ite, *Phys. Rev. Lett.* **2013**, *110*, 083601.
[40] R. S. Tucker, P.-C. Ku, C. J. Chang-Hasnain, *J. Lightwave Technol.* **2005**, *23*, 4046.
[41] T. Pittman, B. Jacobs, J. Franson, *Phys. Rev. A* **2002**, *66*, 042303.
[42] P. P. Rohde, *Phys. Rev. A* **2015**, *91*, 012306.